Article

Fabrication of Nanoporous Gold via an Improved Solid-Phase Method for Non-Enzymatic Detection of Aniline

Qihang Wan [1], Jun Li [1], Zhang Liu [1], Lu Han [1], Siyi Huang [2] and Zumin Wang [1,*

[1]   School of Materials Science and Engineering, Tianjin University, Tianjin 300350, China
[2]   School of Physical Science and Technology, Guangxi University, Nanning 530004, China
*   Correspondence: z.wang@tju.edu.cn

Abstract: In this paper, nanoporous gold (NPG) thin films with superior catalytic performance were prepared on glassy carbon electrodes (GCE) by optimizing the process parameters and adopting an improved solid-phase reaction method. The morphology and structures of NPG films were comprehensively investigated and the structural defects on continuous NPG ligaments were observed. The NPG films demonstrated higher sensitivity and a lower detection limit during the amperometric sensing of aniline than NPGs made using conventional techniques. The results of multiple electrochemical tests demonstrated that the NPG/GCE electrodes possess high stability and good reproducibility. The prepared NPG film is a favorable material that can be superior in aniline electrochemical detection and can also be applied in other electrochemical sensing reactions.

Keywords: NPG; sensor; aniline; electrochemistry

1. Introduction

Aniline is a toxic substance that mainly causes methemoglobinemia, liver, kidney, and skin damage. Besides, aniline is one of the most important intermediates in the dye industry, and is also an important raw material used in the production of many pesticides [1]. In addition, aniline, as an important chemical intermediate, can be used to synthesize various compounds, such as amino compounds, phenolphthalein, etc. More than three billion kilograms of aniline is produced per year worldwide and the demand for this compound is increasing annually [2]. The release of aniline is mainly discharged through underground injection or surface water. The discharge of aniline pollutants in the sewage discharged by the printing and dyeing industry shall not exceed the detection limit, which is less than 0.03 mg/L. Most of the research on aniline detection has been focused on the field of optical sensors, while less research has been carried out on electrochemical sensors. For these reasons, there are many studies aimed at developing reliable aniline assays [3,4]. Therefore, an approach that enables the effective detection of aniline is now urgently needed.

The analytical methods available include a broad spectrum of chemical processes, such as capillary electrophoresis, gas chromatography, liquid chromatography, spectrophotometric methods, and titration [5]. Among the various detection techniques, electrochemical methods are one of the most efficient detections techniques due to their high sensitivity, quick reaction speed, and ease of operation [6–8]. In addition, electrochemical methods are frequently used in chemical analysis, environmental monitoring, biomedicine, and other fields [9]. Therefore, electrochemical detection methods have become one of the indispensable tools in modern chemical analysis. Common electrochemical methods include polarography, linear scanning voltammetry, cyclic voltammetry, etc. Among the many electrochemical detection methods, cyclic voltammetry is widely used in the field of electrochemical analysis because of its advantages of high precision and high sensitivity.

The research on nanoporous metal materials is closely related to the rapid development of many hot fields, such as new energy technology, catalysis, environment, and biological

detection [10]. The continued development of nanoporous metal materials has also led to the widespread use of electrochemical sensors. The biggest expectation of nanotechnology is to harness the size effects of nanomaterials to improve their properties and achieve novel capabilities that are not available from bulk materials. Nanoporous metal materials prepared by solid phase and functionally designed are expected to have great application potential in many important application fields. Nanoporous structure materials have good prospects in catalytics, electric inductance, and actuators, due to the high surface–volume ratio characteristics and abundant surface defects [11–13]. Nanoporous gold is undoubtedly one of the most attractive nanoporous metal materials due to its high electrical conductivity and good stability. The traditional preparation of NPG is a de-alloying method, although the disadvantage of the de-alloying method is that it always leads to the residual of active components, resulting in the waste of materials (especially precious metals). The residuals of these relatively active components and the surface polarization also bring many disturbances and controversies to the study of the intrinsic properties of nanoporous metals. More importantly, the traditional de-alloying method starts with removing a portion of elements from the precursor alloy lattice selectively, which will reduce the volume of the precursor material and then lead to a certain amount of stress. The stress will result in many fine cracks and eventually failure of the NPG. Therefore, one of the most important issues is to find an effective method to prepare large areas of NPG directly on a diversified functional substrate, thus laying a foundation for the universal application of NPG materials in high-tech fields, such as energy conversion and electrocatalysis. Furthermore, relative to the dangerous conventional de-alloying methods of using a strong acid or strong alkali solution in the etching process, it will make great sense to look for a more suitable etcher.

In this work, we prepared NPG films using a modified solid-phase method based on metal-induced crystallization (MIC) theory [14–16]. First, we deposited a three-layer Ge/Au/Ge precursor film on a functional substrate using a high-vacuum magnetron sputtering device. Subsequently, Ge was etched with a low concentration of hydrogen peroxide to obtain NPG films with a nanoporous mesh structure. Then, we performed a series of electrochemical tests with the prepared NPG/GCE electrode and found that it exhibited good catalytic performance for the electrochemical detection of aniline.

2. Experimental Methods

2.1. Materials

Aniline, HF, H_2SO_4, CH_3COOH, H_3BO_3, H_3PO_4, NaOH, and H_2O_2, of analytical grade, were produced by Tianjin Yuanli Chemical Company, and all substances were used without any further purification. Britton-Rob buffer solution (BR) was prepared by mixing 0.04 mol/L of CH_3COOH, H_3BO_3, and H_3PO_4, and adding 0.2 mol/L of NaOH solution to adjust the pH of the solution. The BR buffer solutions with pH 6.8, 7.0, 7.2, 7.4, 7.6, and 7.8 were prepared. Ultrapure water was purchased from Shanghai Aladdin Biochemical Technology.

2.2. Fabrication of NPG

A schematic flowchart of the manufacturing process of NPG films on a glass-carbon electrode is shown in Figure 1. A tri-layer of amorphous Ge (a-Ge), Au, and a-Ge was deposited on the glass-carbon electrodes by magnetron sputtering, respectively. Magnetron sputtering was performed in a high-vacuum environment (base pressure $\leq 10^{-5}$ Pa). The substrates were glass-carbon electrodes (for electrochemical analysis) and Si wafers covered with an amorphous SiO_2 of 50 nm (for the subsequent observation), respectively. The substrate was cleaned for twenty minutes using successive ultrasonic treatments in acetone, ethanol, and ultrapure water, respectively. Before sputtering, the substrate was washed with Ar^+ in the vacuum chamber for 10 min. The films of Ge and Au were deposited by sputtering from a pure Ge target (purity 99.99 wt. %) and a pure Au target (purity 99.99 wt. %) at 110 °C, with the radio frequency of 64 W and direct current of 16 W, respectively. The thickness of the sputtered layers at different sputtering times

at specific sputtering pressures was measured using the profilometer (Wuhan Optical Instruments). Thus, the deposition rates of the film layers at different sputtering pressures were determined by fitting a linear function between the film thicknesses of Au and Ge, respectively, and the corresponding sputtering times. The substrate was first covered with a 5 nm-thick Ge sublayer, and then a 20 nm-thick Au sublayer was deposited on the bottom Ge layer. Finally, a 35 nm a-Ge layer was deposited on the Au film. The sputtering pressures of the A-Ge/Au/a-Ge layers were 0.6 Pa, 3 Pa, and 1.2 Pa, respectively. The deposition rates of the a-Ge and Au were 11.8 nm/min and 3.4 nm/min, respectively. The improved solid-phase method simplifies the process steps and saves costs by conducting the annealing process simultaneously with the sputtering process in a vacuum chamber. The in-suit annealing process can promote the MIC process, and the mesh-like nanostructures were developed by the reciprocal migration of Au and Ge atoms [17–19]. During magnetron sputtering, the substrate was continuously rotated at 20 rpm to ensure the uniformity of the thin films. The prepared precursor films were first cleaned with deionized water to remove any possible contamination during storage, and then they were etched with 30 vol. % H_2O_2 using a dropper until submerged, and the Ge was selectively etched off by etching for 7 min. Finally, the surface was dried with a nitrogen gun and the electrode was stored under a vacuum.
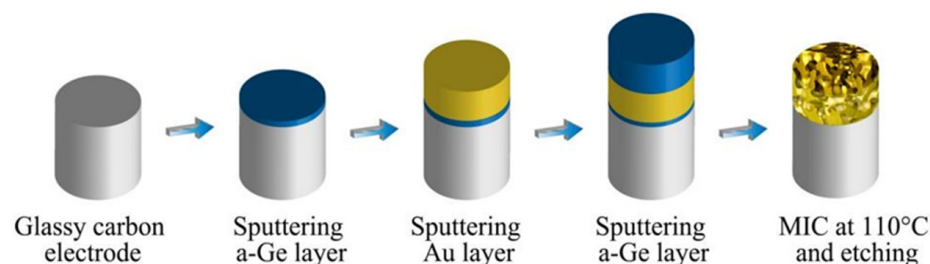

Figure 1. A schematic depicting the manufacturing process for NPGs on glassy carbon electrodes.

The mechanism of NPG formation can be explained by the theory of metal-induced crystallization. MIC is the theory that contact between an amorphous semiconductor and a metal induces crystallization of an amorphous semiconductor at a very low temperature. The essence of MIC is a phase transition phenomenon from solid to solid that occurs at the surface or interface within the thin-film system. MIC theory can be applied to many important fields, such as solar cells, semiconductor devices, displays, sensors, and biomedical applications. Specifically, when a-Ge layer is in contact with the Au layer interface, A-Ge can migrate along the grain boundaries to the Au layer at a very low temperature, and subsequently nucleate and grow on the grain boundaries, which leads to increased compressive stresses within the Au layer and increased tensile stresses within the a-Ge layer. The resulting stress gradient leads to further solid-state transport from the Au layer to the a-Ge, ultimately resulting in the exchange of film layers. After etching, an NPG film with a nanoporous mesh structure was formed. Ge was chosen as the target because it is easily etched by low concentrations of hydrogen peroxide in amorphous semiconductor materials and the whole etching process is safer and more harmless than the conventional etching process.

2.3. Characterizations of NPG

Scanning electron microscopy and energy-dispersive spectroscopy (EDS) examinations were carried out using a Hitachi S-4800 microscope with an applied voltage set at 5 kV. The average ligament size was calculated according to the measurements of 500 distinct ligaments in SEM micrographs. Transmission electron microscopy (TEM) was performed on a JEM-2100F microscope with an acceleration voltage of 200 kV. The etched precursor film was submerged in HF and the NPG film was peeled off from the silicon substrate. The NPG film floating on the surface was carefully dipped into the toothpick and mixed with anhydrous ethanol to form a certain proportion of suspension. The suspension was

sonicated with an ultrasonicator until it was uniformly dispersed and then titrated onto the copper network, which can be used for TEM observation after drying.

2.4. Electrochemical Analysis

An electrochemical workstation (CHI 660E, purchased from Beijing Huake Putian Technology Company) was used for all electrochemical tests at 25 °C [20–22]. Glass-carbon electrodes were used as the substrates of a three-electrode system, consisting of the working (3 mm-diameter NPG/GCE), reference (saturated calomel electrode, SCE), and counter electrodes (platinum wire). A 20 nm-thin layer of polycrystalline gold was deposited on the glassy carbon electrode using the same magnetron sputtering process and under the same process parameters as described in Section 2.2. The prepared Au/NPG electrode and bare glassy carbon electrode can be used for electrochemical experiments of non-enzymatic detection of aniline and compared with the performance of the NPG/GCE electrode. Before constructing the NPG/GCE and Au/GCE electrodes, the glassy carbon electrode was uniformly polished with a polishing cloth with 0.5 and 0.05 mm alumina suspension in turn. The polishing process should ensure that the electrode surface is flat and the polishing force should be appropriate not to damage the electrode surface. After polishing, the electrode surface was ultrasonically cleaned with deionized water and anhydrous ethanol for 15 min. Before electrochemical testing, 15 cycles of electrochemical cyclic voltammetry were applied to the NPG/GCE electrode in BR buffer solution to activate the electrode, all electrolytes underwent a minimum of 30 min of nitrogen bubbling (purity 99.999 vol. %) deoxygenation, and all experiments were carried out at room temperature.

3. Results and Discussion

The morphology of the as-prepared NPG film is shown in Figure 2a. The grain size of the film is nanoscale. According to the EDS analysis, in addition to the composition of the substrate Si, the atomic ratio of Ge (12.7 at. %) and Au (13 at. %) in the film was close to 2 (see Figure 2d). After etching, the film demonstrated a typical bi-continuous porous structure at different magnifications (Figure 2b,c) [23–25]. The EDS analysis in Figure 2e reveals that the Ge atoms were completely removed after etching. The distribution of the ligament width was consistent with the normal distribution, which shows a good Gaussian curve fit, and the calculated ligament width of NPG was about 28 nm (Figure 2f). Due to the unique structure of NPG, the surface and volume ratio were high, resulting a great advantage for high-sensitivity detection of aniline.
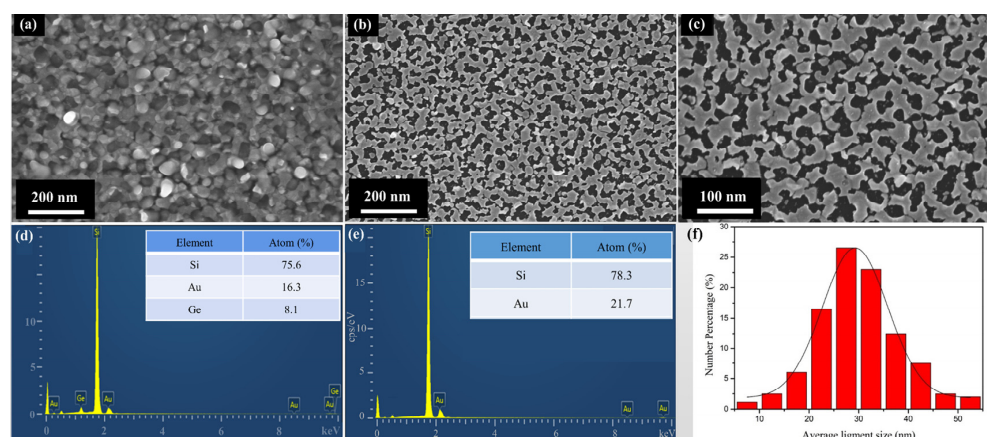

Figure 2. SEM images of the morphology of as-prepared NPG film (**a**) before and (**b,c**) after etching, the corresponding EDS analyses of the NPG (**d**) before and (**e**) after etching, and (**f**) the distribution of ligament diameters.

Figure 3 shows the SEM image and the corresponding EDS mappings of the NPG thin film after etching. The result indicates a nanoporous structure in the etching film, which

consisted of Au ligaments. The Si element was abundantly distributed in the whole scanned area, which was because the prepared porous gold film layer was very thin and the SEM mapping results could detect the Si element from the silicon substrate. The distribution of Ge elements was sparse and scattered. Combined with the results of the quantitative elemental analysis in Figure 2d, it can be indicated that Ge elements were completely removed after the etching of the NPG precursor film.
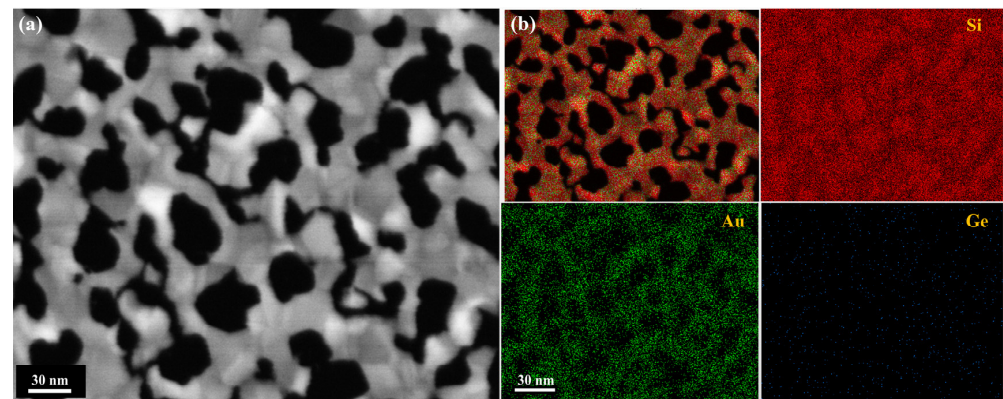

Figure 3. (**a**) SEM image of NPG thin film after etching and (**b**) the corresponding EDS mappings of NPG thin film.

Figure 4a,b show the TEM images of NPG at different magnifications. The results show that the porous structure of the films could reach the nanoscale level and the nanoporous gold ligaments were uniformly distributed, and this microstructure, consisting of curved ligaments and abundant pore channels, will lead to a large specific surface area of the NPG films, which will improve the electrocatalytic performance of the NPG. The diffraction rings of Au in the corresponding diffraction pattern (see Figure 4c) reveal that the prepared NPG was polycrystalline. The high-resolution transmission electron microscope (HRTEM) images of the NPG are shown in Figure 4d–f. The results demonstrate that the NPG had several common structural defects, including grain boundaries (Figure 4d), stacking faults (Figure 4e), and twins (Figure 4f). The high density of defects in the NPG favors the improved catalytic performance of NPG. The formation of these defects is related to a large number of low-coordination atoms on NPG. These defects can serve as catalytic active sites to facilitate the catalytic process [26–28].
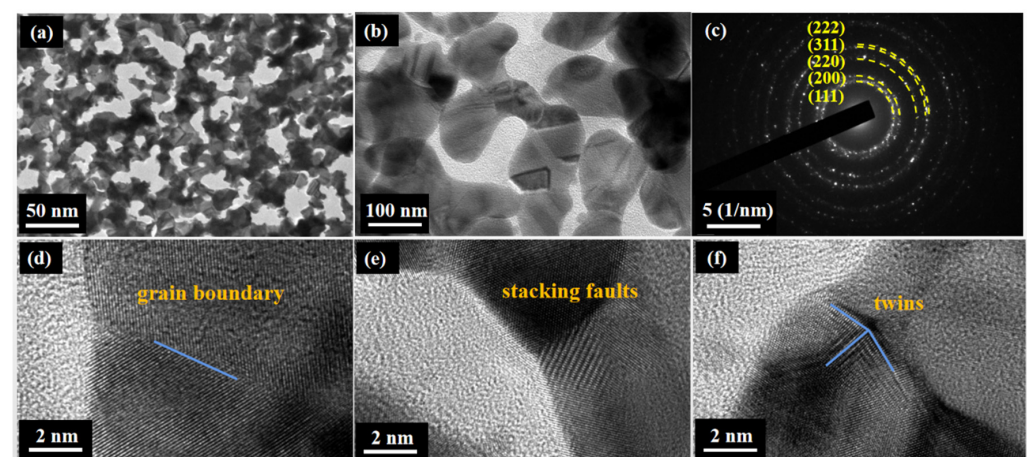

Figure 4. (**a**,**b**) TEM images of the microstructure of the NPG thin film and (**c**) the appropriate SAED pattern. HRTEM images of the NPG thin film show the following surface flaws: (**d**) grain boundaries, (**e**) stacking faults, and (**f**) twins.

The cyclic voltammetric curve of the prepared NPG with a representative CV curve at a scan rate of 100 mV·s^{-1}, from 0.25 V to 1.80 V, is shown in Figure 5 (The arrow represents the direction of potential scanning). Before the test, ten CV cycles were run to guarantee the stability of the test. The Au atoms at the surface were more active than that in the bulk, and thus the oxidation of Au took place during the positive sweep at a voltage lower than E^0 (Au + 3H$_2$O = Au$_2$O$_3$ + 6H$^+$ + 6e$^-$, E^0 = 1.46 V), at around 1.1 V [29]. It was found that the reducing peak occurred at about 0.9 V, and the integral area of the reduction peak can be used to calculate the electrochemically active surface area of the NPG electrode. During the cyclic voltammetry test process, gold can be oxidized into gold ions when the potential of a rotating disk gold electrode exceeds 1.13 V, and most of the ions combined with O to form Au$_2$O$_3$ on the electrode surface. The formed Au$_2$O$_3$ at the surface was insoluble during the test process. However, there were also a small amount of gold ions without O bonding that dissolved into the sulfuric acid solution and contributed to part of the anodic charge to the oxidation peak [30–32]. With the dissolution of these gold ions, they do not contribute to the total charge during the reduction peak, and therefore the electrochemically active surface area was calculated by the reduction peak [33,34]. The measured electrochemically active surface area was 0.41 cm^2, which is far greater than the geometric surface area (0.19 cm^2) and larger than the area prepared with previous process parameters (0.33 cm^2) [35].
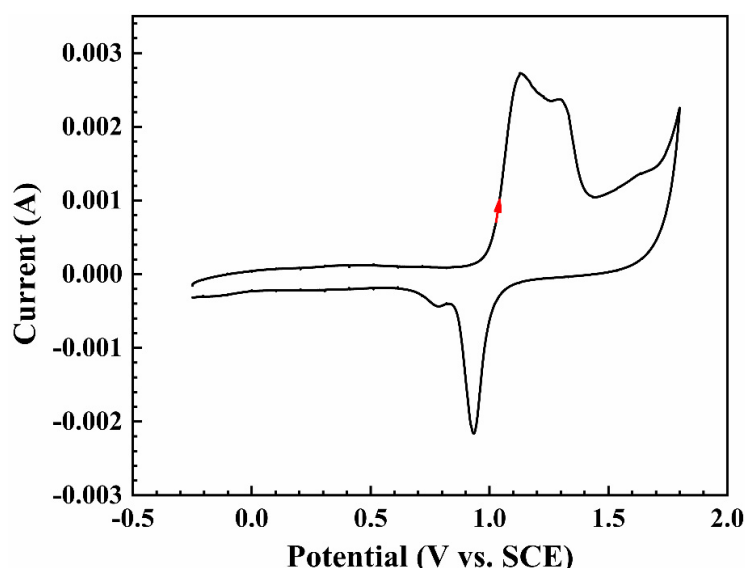

Figure 5. Cyclic voltammetric curve of NPG films in a 0.5 M H$_2$SO$_4$ solution.

The CV curve recorded in a buffer with (0.5 mM) and without aniline was obtained under the potential of −0.2 V to 1.6 V, and the scan rate of 100 mV s^{-1} (see Figure 6a, the arrow represents the direction of potential scanning). It follows that there was no redox peak in the NPG electrode without the added aniline buffer solution, whereas, an obvious oxidation peak appeared at about 0.9 V after the addition of 0.5 mM of aniline. The results above indicated that the NPG electrode can effectively detect aniline. In addition, the oxidation of aniline involving multiple complex reactions that produce polymer attachment to the electrode surface resulted in the absence of a reduction peak. Furthermore, aniline undergoes oxidation to produce a free radical, which readily dimerizes to form benzidine or p-amino diphenylamine. As a result, the polymer on the electrode surface can be removed by increasing the potential [36]. Figure 6b shows the cyclic voltammetric characteristic curves of NPG/GCE, Au/GCE, and GCE electrodes in BR buffer solution with 0.5 mM of aniline added. The results show that the peak currents of the NPG/GCE and Au/GCE electrodes for the detection of aniline were higher than those measured with the pure GCE electrode, which indicates that gold can improve the electrochemical performance of the GCE electrode for the detection of aniline. The peak currents measured with the

NPG/GCE electrode were much higher than those with the Au/GCE electrode, indicating that NPG exhibited a higher catalytic performance for the electrochemical detection of aniline compared to pure gold materials. The superior catalytic performance of NPG is related to its higher electrocatalytic active surface area and more catalytic active site.
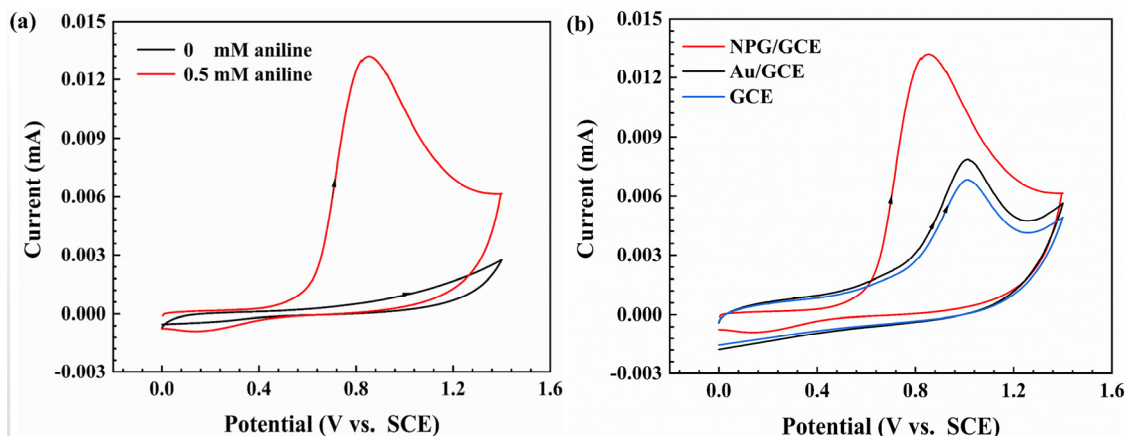

Figure 6. (**a**) Cyclic voltammetric curve of an NPG film in BR buffer solution with and without 0.5 mM of aniline. (**b**) Cyclic voltammetric curves of NPG/GCE, Au/GCE, and GCE electrodes measured in BR buffer solution with 0.5 mM of aniline.

Figure 7a shows the relationship between the peak current and the electrode rotation speed. The peak current (measured at 0.9 V) was measured in the solution with 0.5 mM of buffer at 100 mV·s^{-1}. The peak current increased and reached the maximum peak current when the rotation speed reached 1400 rpm, and then it decreased as the electrode rotation speed increased. As the rotation speed increased, the distance of the diffusion layer of the solute decreased, the diffusion rate of the reactant increased, and the peak current increased. With the further increase of the electrode rotation speed, the peak current decreased instead. Although the diffusion rate of the reactant continued to increase, the too-fast rotation speed of the electrode led to the convection of the solution, and generated high shear stress [37]. The process of polymerization of aniline oxidation products on the surface, thus leading to a decrease in the peak current, was accelerated. In order to obtain the optimum experimental conditions under neutral solution conditions, the relationship between the peak current and pH was investigated within the neutral pH range. Figure 7b shows that the peak current reached a maximum at the pH of 7.2. Therefore, all subsequent experiments were performed at speeds of 1400 rpm and a pH of 7.4.
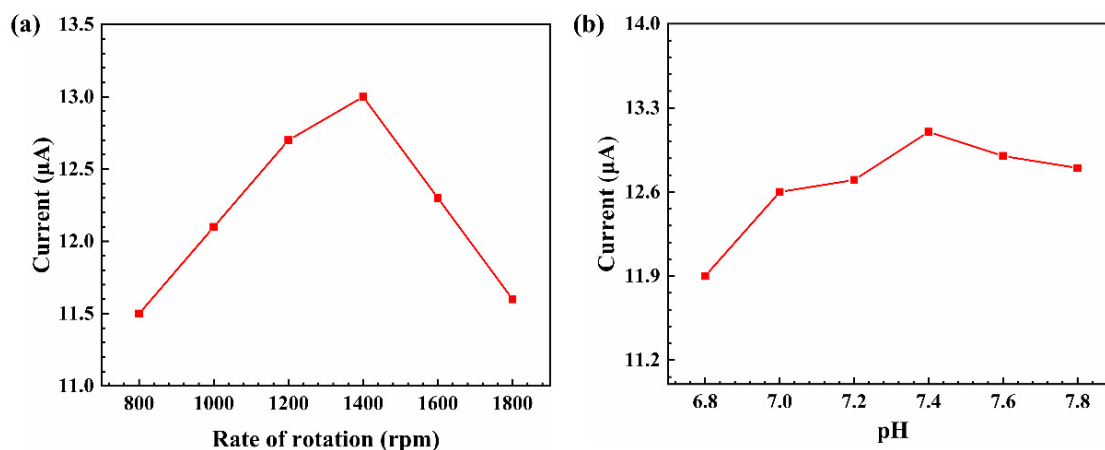

Figure 7. (**a**) The peak current measured in multiple experiments with the electrode rotation velocity from 800 to 1800 rpm, and (**b**) different pH levels, from 6.8 to 7.8.

Figure 8a shows the relationship between the electrode scan rate and the peak current generated by the oxidation of aniline, and the CV curves were measured in BR buffer solution supplemented with 0.5 mM of aniline at an electrode scan rate from 5 mV s^{-1} to 100 mV s^{-1}. The peak potential moved somewhat in the positive direction with the increased scanning rate. As demonstrated in Figure 8b, the peak current of aniline oxidation and the square root of the scanning rate ($v^{1/2}$) had a linear relationship. The result indicates that the aniline oxidation on the NPG electrode is a typical diffusion control process [38,39].
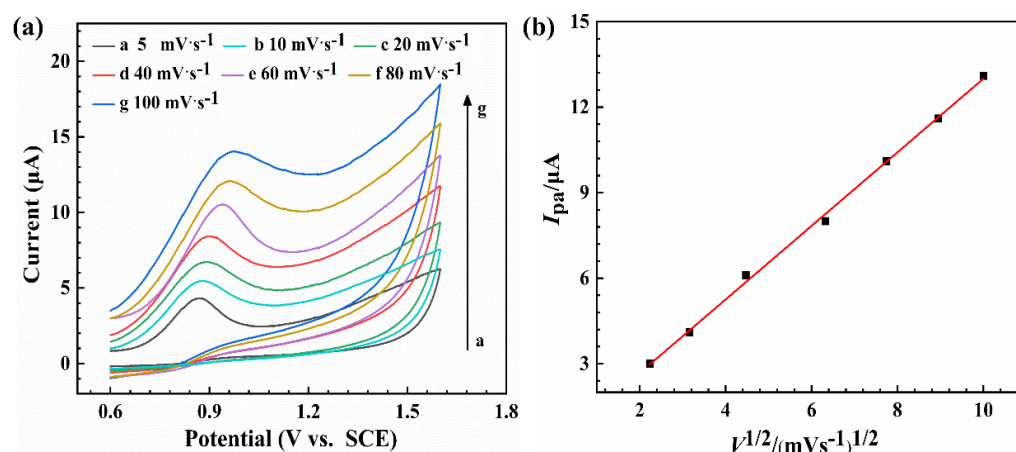

Figure 8. (**a**) CV curves obtained with 0.5 mM of aniline in buffer solution (pH = 7.4) on NPG with different scan rates from 5 to 100 mV s^{-1}. (**b**) Plot of peak current against $v^{1/2}$.

The partial CV curves obtained in a buffer solution with different concentrations of aniline are shown in Figure 9a. The ampere current response was measured at different concentrations of aniline at 0.9 V. Before the test, five cycles were performed to ensure the stable response current and the reliability of results. There was a linear relationship between aniline concentration and current (Figure 9b). The sensitivity was measured as 450 nA μM^{-1}. The limit of detection (LOD) was found to be 0.5 μM with a signal-to-noise ratio of 3 (S/N = 3). The comparison of the performance of non-enzymatic electrochemical sensors constructed with the NPG/GCE electrode and other electrode materials regarding aniline detection is summarized in Table 1 [3,4,36]. The NPG/GCE electrode developed in this work showed a higher sensitivity for aniline compared to previously reported electrodes. This excellent electrocatalytic performance of NPG/GCE is associated with the large active surface area and the large number of surface defects generated using an improved solid-phase reaction method (see Figure 3).
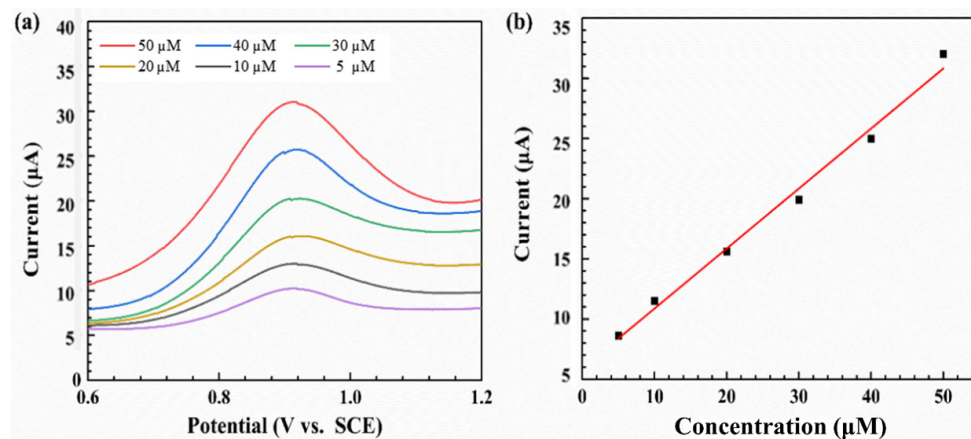

Figure 9. Performance of the NPG in the BR buffer solution. (**a**) Current response with serial additions of 10 μM of aniline into the BR buffer solution, and (**b**) plot of peak current against aniline concentration.

Table 1. The performances of aniline sensors prepared in this work and in previous works [3,4,36].

Electrode	Sensitivity (nA μM^{-1})	LOD (μM)	Peak Potential (V)	Ref.
BBD	310	3.0	0.95	[36]
Nanoporous gold	350	0.5	0.80	[3]
NP-Au	207	0.5	1.10	[4]
NPG/GCE	480	0.5	0.90	this work

Figure 10a shows the peak currents of the same electrode at different times of cyclic voltammetry tests, and the tests were performed in a buffer solution supplemented with 0.5 mM of aniline. It was found that the peak current decreased by less than 6% after 25 cycles of voltammetric tests compared with 5 cycles of the test, which indicates that the prepared NPG/GCE electrode has good stability. Figure 10b presents the peak currents of NPG electrodes prepared with the same preparation parameters after 5 cycles of voltammetric tests and numbered as electrodes 1–5, respectively. The relative standard deviation of peak current was calculated by 3%, indicating that the performance exhibited by electrochemical detection of aniline with NPG/GCE electrodes is reproducible. Figure 10a,b illustrate that the prepared NPG/GCE electrodes have good reproducibility and stability. The good reproducibility and stability of NPG/GCE electrodes are attributed to the stable structure and the stability of gold [40,41].
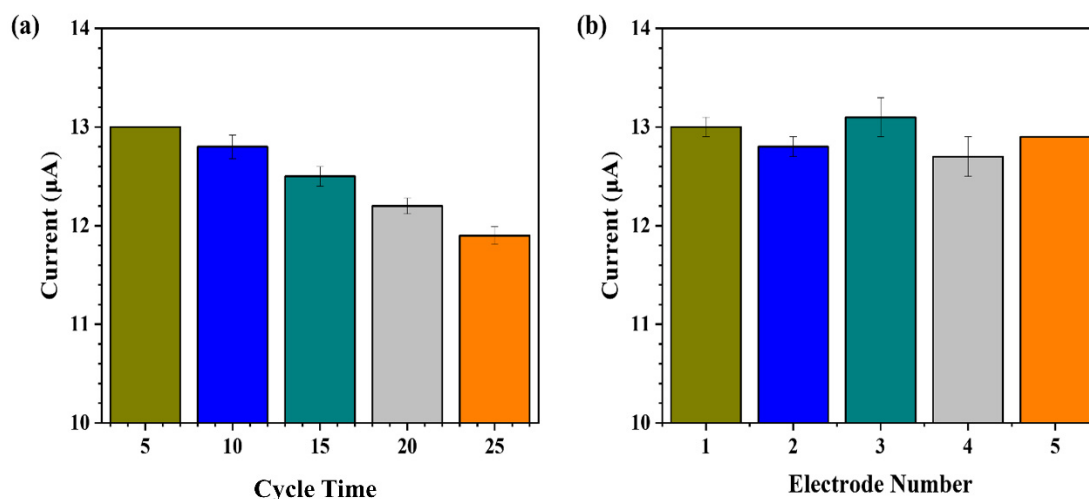

Figure 10. Peak current of (**a**) the prepared NPG/GCE electrode under voltammetry tests with different times of cycles (5, 10, 15, 20, 25), and (**b**) every NPG/GCE electrode (numbered 1–5) after 5 cycles of voltammetry testing.

4. Conclusions

The NPG/GCE electrode with good electrochemical properties was prepared on the glass-carbon electrode by using an improved solid-phase reaction method on the basis of the MIC process. The aniline detection capabilities of NPG thin films as aniline detection sensors were investigated, and the prepared NPG/GCE electrode was found to exhibit higher electrochemical catalytic performance compared to the Au/GCE and GCE electrodes for electrochemical, non-enzymatic detection of aniline. In addition, the prepared NPG/GCE electrodes exhibited higher sensitivity and lower detection limits and showed good stability and reproducibility. The huge active surface area and distinctive structure of multiple defects of the sensor led to its remarkable electrochemical performance. In this work, a method was developed to prepare the environment-friendly NPG sensors as promising applications in the field of electric inductance.

Data Availability Statement: Not applicable.

Conflicts of Interest: The authors declare no conflict of interest.

References

1. Mitadera, M.; Spataru, N.; Fujishima, A. Electrochemical oxidation of aniline at boron-doped diamond electrodes. *J. Appl. Electrochem.* **2004**, *34*, 249–254. [CrossRef]
2. Zhang, L.M.; Li, B. A highly selective optical sensor for aniline recognition. *Spectrochim. Acta Part A-Mol. Biomol. Spectrosc.* **2009**, *74*, 1060–1063. [CrossRef] [PubMed]
3. Quynh, B.T.P.; Byun, J.Y.; Kim, S.H. Nanoporous gold for amperometric detection of amino-containing compounds. *Sens. Actuators B Chem.* **2014**, *193*, 1–9. [CrossRef]
4. Lee, K.-U.; Tran, T.H.; Kim, S.H.; Shin, H.-J. Fabrication of nanoporous gold thin films on glass substrates for amperometric sensing of aniline. *J. Alloys Compd.* **2017**, *713*, 132–137. [CrossRef]
5. Zambonin, C.G.; Quinto, M.; De Vietro, N.; Palmisano, F. Solid-phase microextraction—Gas chromatography mass spectrometry: A fast and simple screening method for the assessment of organophosphorus pesticides residues in wine and fruit juices. *Food Chem.* **2004**, *86*, 269–274. [CrossRef]
6. Park, S.; Kim, H.C.; Chung, T.D. Electrochemical analysis based on nanoporous structures. *Analyst* **2012**, *137*, 3891–3903. [CrossRef]
7. Xia, Y.; Huang, W.; Zheng, J.; Niu, Z.; Li, Z. Nonenzymatic amperometric response of glucose on a nanoporous gold film electrode fabricated by a rapid and simple electrochemical method. *Biosens. Bioelectron.* **2011**, *26*, 3555–3561. [CrossRef]
8. Yan, X.; Meng, F.; Cui, S.; Liu, J.; Gu, J.; Zou, Z. Effective and rapid electrochemical detection of hydrazine by nanoporous gold. *J. Electroanal. Chem.* **2011**, *661*, 44–48. [CrossRef]
9. Xu, C.; Xu, X.; Su, J.; Ding, Y. Research on unsupported nanoporous gold catalyst for CO oxidation. *J. Catal.* **2007**, *252*, 243–248. [CrossRef]
10. Zhang, X.M.; Ding, Y. Unsupported nanoporous gold for heterogeneous catalysis. *Catal. Sci. Technol.* **2013**, *3*, 2862–2868. [CrossRef]
11. Russell, A.E. Electrocatalysis: Theory and experiment at the interface. Preface. *Faraday Discuss.* **2008**, *140*, 9–10. [CrossRef] [PubMed]
12. Sukeri, A.; Lima, A.S.; Bertotti, M. Development of non-enzymatic and highly selective hydrogen peroxide sensor based on nanoporous gold prepared by a simple unusual electrochemical approach. *Microchem. J.* **2017**, *133*, 149–154. [CrossRef]
13. Verma, N. A green synthetic approach for size tunable nanoporous gold nanoparticles and its glucose sensing application. *Appl. Surf. Sci.* **2018**, *462*, 753–759. [CrossRef]
14. Wang, Z.M.; Wang, J.Y.; Jeurgens, L.P.H.; Mittemeijer, E.J. Thermodynamics and mechanism of metal-induced crystallization in immiscible alloy systems: Experiments and calculations on Al/a-Ge and Al/a-Si bilayers. *Phys. Rev. B* **2008**, *77*, 045424. [CrossRef]
15. Wang, Z.M.; Wang, J.Y.; Jeurgens, L.P.H.; Phillipp, F.; Mittemeijer, E.J. Origins of stress development during metal-induced crystallization and layer exchange: Annealing amorphous Ge/crystalline Al bilayers. *Acta Mater.* **2008**, *56*, 5047–5057. [CrossRef]
16. Wang, Z.M.; Gu, L.; Phillipp, F.; Wang, J.Y.; Jeurgens, L.P.H.; Mittemeijer, E.J. Metal-Catalyzed Growth of Semiconductor Nanostructures Without Solubility and Diffusivity Constraints. *Adv. Mater.* **2011**, *23*, 854–859. [CrossRef]
17. Van Gestel, D.; Gordon, I.; Poortmans, J. Metal induced crystallization of amorphous silicon for photovoltaic solar cells. In Proceedings of the Asia-Pacific Conference on Semiconducting Silicides Science and Technology Towards Sustainable Optoelectronics (APAC-SILICIDE), Tsukuba, Japan, 24–26 July 2010; pp. 196–199.
18. Konno, T.J.; Sinclair, R. Metal-contact-induced crystallization of semiconductors. *Mater. Sci. Eng. A Struct. Mater. Prop. Microstruct. Process.* **1994**, *179–180*, 426–432. [CrossRef]
19. Katsuki, F.; Hanafusa, K.; Yonemura, M.; Koyama, T.; Doi, M. Crystallization of amorphous germanium in an Al/a-Ge bilayer film deposited on a SiO2 substrate. *J. Appl. Phys.* **2001**, *89*, 4643–4647. [CrossRef]
20. Lang, X.Y.; Fu, H.Y.; Hou, C.; Han, G.F.; Yang, P.; Liu, Y.B.; Jiang, Q. Nanoporous gold supported cobalt oxide microelectrodes as high-performance electrochemical biosensors. *Nat. Commun.* **2013**, *4*, 2169. [CrossRef] [PubMed]
21. Rosner, H.; Parida, S.; Kramer, D.; Volkert, C.A.; Weissmuller, J. Reconstructing a nanoporous metal in three dimensions: An electron tomography study of dealloyed gold leaf. *Adv. Eng. Mater.* **2007**, *9*, 535–541. [CrossRef]
22. Heller, A.; Feldman, B. Electrochemical glucose sensors and their applications in diabetes management. *Chemical Reviews* **2008**, *108*, 2482–2505. [CrossRef] [PubMed]
23. El-Said, W.A.; Lee, J.-H.; Oh, B.-K.; Choi, J.-W. 3-D nanoporous gold thin film for the simultaneous electrochemical determination of dopamine and ascorbic acid. *Electrochem. Commun.* **2010**, *12*, 1756–1759. [CrossRef]

24. Tang, Y.Y.; Kao, C.L.; Chen, P.Y. Electrochemical detection of hydrazine using a highly sensitive nanoporous gold electrode. *Anal. Chim. Acta* **2012**, *711*, 32–39. [CrossRef]

25. Wu, B.; Zheng, N. Surface and interface control of noble metal nanocrystals for catalytic and electrocatalytic applications. *Nano Today* **2013**, *8*, 168–197. [CrossRef]

26. Biener, J.; Wittstock, A.; Zepeda-Ruiz, L.A.; Biener, M.M.; Zielasek, V.; Kramer, D.; Viswanath, R.N.; Weissmuller, J.; Baumer, M.; Hamza, A.V. Surface-chemistry-driven actuation in nanoporous gold. *Nat. Mater.* **2009**, *8*, 47–51. [CrossRef]

27. Gupta, G.; Thorp, J.C.; Mara, N.A.; Dattelbaum, A.M.; Misra, A.; Picraux, S.T. Morphology and porosity of nanoporous Au thin films formed by dealloying of AuxSi1−x. *J. Appl. Phys.* **2012**, *112*, 094320. [CrossRef]

28. Fujita, T.; Guan, P.; McKenna, K.; Lang, X.; Hirata, A.; Zhang, L.; Tokunaga, T.; Arai, S.; Yamamoto, Y.; Tanaka, N.; et al. Atomic origins of the high catalytic activity of nanoporous gold. *Nat. Mater.* **2012**, *11*, 775–780. [CrossRef] [PubMed]

29. Wittstock, A.; Biener, J.; Baumer, M. Nanoporous gold: A new material for catalytic and sensor applications. *Phys. Chem. Chem. Phys.* **2010**, *12*, 12919–12930. [CrossRef]

30. Cadle, S.H.; Bruckenstein, S. Ring-disk electrode study of the anodic behavior of gold in 0.2M sulfuric acid. *Anal. Chem.* **1974**, *46*, 16–20. [CrossRef]

31. Tian, M.; Pell, W.G.; Conway, B.E. Nanogravimetry study of the initial stages of anodic surface oxide film growth at Au in aqueous HClO4 and H2SO4 by means of EQCN. *Electrochim. Acta* **2003**, *48*, 2675–2689. [CrossRef]

32. Jusys, Z.; Bruckenstein, S. Electrochemical quartz crystal microgravimetry of gold in perchloric and sulfuric acid solutions. *Electrochem. Solid State Lett.* **1998**, *1*, 74–76. [CrossRef]

33. Do, U.P.; Seland, F.; Johannessen, E.A. The Real Area of Nanoporous Catalytic Surfaces of Gold and Palladium in Aqueous Solutions. *J. Electrochem. Soc.* **2018**, *165*, H219–H228. [CrossRef]

34. Li, Z.G.; Zhang, L.L.; Zeng, S.L.; Zhang, M.H.; Du, E.M.; Li, B.L. Effect of surface pretreatment on self-assembly of thiol-modified DNA monolayers on gold electrode. *J. Electroanal. Chem.* **2014**, *722*, 131–140. [CrossRef]

35. Yang, Z.P.; Li, J.; Liu, P.M.; Zhang, A.; Wang, J.; Huang, Y.; Wang, J.Y.; Wang, Z.M. Highly sensitive non-enzymatic hydrogen peroxide monitoring platform based on nanoporous gold via a modified solid-phase reaction method. *Rsc. Adv.* **2021**, *11*, 36753–36759. [CrossRef]

36. Spataru, T.; Spataru, N.; Fujishima, A. Detection of aniline at boron-doped diamond electrodes with cathodic stripping voltammetry. *Talanta* **2007**, *73*, 404–406. [CrossRef]

37. Ashassi-Sorkhabi, H.; Asghari, E. Electrochemical corrosion behavior of Al7075 rotating disc electrode in neutral solution containing l-glutamine as a green inhibitor. *J. Appl. Electrochem.* **2010**, *40*, 631–637. [CrossRef]

38. Collinson, M.M. Nanoporous Gold Electrodes and Their Applications in Analytical Chemistry. *ISRN Anal. Chem.* **2013**, *2013*, 692484. [CrossRef]

39. Quynh, B.T.P.; Byun, J.Y.; Kim, S.H. Non-enzymatic amperometric detection of phenol and catechol using nanoporous gold. *Sens. Actuators B Chem.* **2015**, *221*, 191–200. [CrossRef]

40. Ke, X.; Li, Z.; Gan, L.; Zhao, J.; Cui, G.; Kellogg, W.; Matera, D.; Higgins, D.; Wu, G. Three-dimensional nanoporous Au films as high-efficiency enzyme-free electrochemical sensors. *Electrochim. Acta* **2015**, *170*, 337–342. [CrossRef]

41. Zielasek, V.; Jurgens, B.; Schulz, C.; Biener, J.; Biener, M.M.; Hamza, A.V.; Baumer, M. Gold catalysts: Nanoporous gold foams. *Angew. Chem. Int. Ed. Engl.* **2006**, *45*, 8241–8244. [CrossRef] [PubMed]